tion. Alternatively, as the Mendocino triple junction passed, a "tectonic snow plow" created by the differential topography of juxtaposed old and young oceanic lithosphere at a transform fault may be a credible driving mechanism, depending on the depth to which such a feature might persist.

References and Notes

1. J. G. Moore, *J. Geol.* **67**, 197 (1959).
2. J. F. Evernden and R. W. Kistler, *U.S. Geol. Surv. Prof. Pap.* 623 (1970).
3. R. W. Kistler and Z. E. Peterman, *U.S. Geol. Surv. Prof. Pap.* 1071 (1973).
4. D. C. Ross, *U.S. Geol. Surv. Open File Rep. 80-307* (1980).
5. A. Locke, *Geol. Soc. Am. Bull.* **51**, 513 (1940).
6. B. C. Burchfiel and G. A. Davis, in *The Geotectonic Development of California*, W. G. Ernst, Ed. (Prentice-Hall, Englewood Cliffs, N.J., 1981), pp. 217–252.
7. L. R. Kanter and M. McWilliams, *J. Geophys. Res.* **87**, 3819 (1982).
8. B. Turrin, unpublished data.
9. M. McWilliams, *Rev. Geophys. Space Phys.* **21**, 644 (1983).
10. J. G. Vedder, D. G. Howell, J. A. Forman, *Soc. Econ. Paleontol. Minerol. Pacific Sect. Paleogeogr. Symp.* **3**, 239 (1979).
11. L. S. Frei, J. R. Magill, A. Cox, *Tectonics* **3**, 157 (1984).
12. R. S. Stein and W. Thatcher, *J. Geophys Res.* **86**, 4913 (1981).
13. T. M. Harrison and K. Bé, *Earth Planet. Sci. Lett.* **64**, 244 (1983).
14. J. L. Burnett, *California Division of Mines and Geology Map Sheet 35* (1976).
15. M. E. Beck, *Tectonophysics* **93**, 1 (1983).
16. B. M. Page and D. C. Engebretson, *Tectonics* **3**, 133 (1984).
17. T. H. Nilsen, *Soc. Econ. Paleontol. Minerol. Pacific Sect. Field Trip Guideb.* **2**, 7 (1973).
18. M. McWilliams, *Geophys. Res. Lett.* **11**, 825 (1984).
19. We thank M. Fones, P. Layer, and J. Tarduno for help with sample collection; D. Ross for advice on site selection and preprints of geological maps; and M. Basher of the California Department of Water Resources for permission to collect samples. Supported by NSF and the Petroleum Research Fund.

20 September 1984; accepted 12 July 1985

content (*3*). We now report the discovery of dust devils in Viking Orbiter images; this finding provides an important documentation of a specific form of dust entrainment by winds on Mars.

Dust devils have meteorological as well as geological significance. Fluid motions in an atmospheric boundary layer can be driven either by stresses due to the mean wind (forced convection) or by buoyancy due to heating of the gas adjacent to the surface (free convection) (*4*). Dust devils are an example of the latter. On Earth, large-scale eolian transport is generally due to forced convection. Moderate to high winds characterize forced convection, and on Mars, where the atmospheric density is only about 1 percent of that on Earth, it is estimated that winds must exceed about 25 to 40 m sec^{-1} to initiate soil movement (*5*). Because near-surface winds this strong are rare (*6*), it is of great interest to discover that other modes of dust entrainment are acting.

Small bright clouds with long, tapered shadows (Fig. 1), distinctive forms among the many albedo and atmospheric features observed on Mars, were initially found during mapping of linear wind streaks in Amazonis Planitia. A search was then made of all Viking Orbiter images for other dust devils. Criteria for positive identification of a feature as a dust devil were (i) an elongated shape, (ii) a nearly vertical orientation, and (iii) transience. The first two criteria rule out cumulus clouds or streaks of windblown
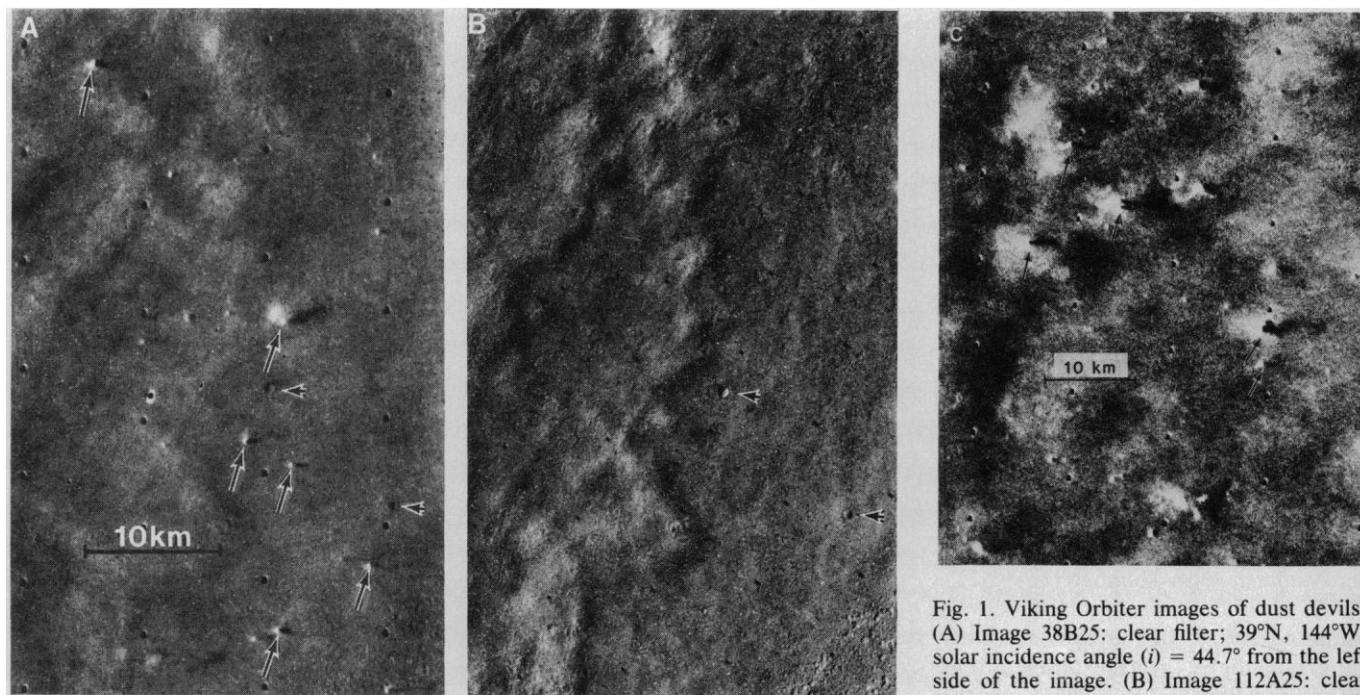
Dust Devils on Mars

Abstract. *Columnar, cone-shaped, and funnel-shaped clouds rising 1 to 6 kilometers above the surface of Mars have been identified in Viking Orbiter images. They are interpreted as dust devils, confirming predictions of their occurrence on Mars and giving evidence of a specific form of dust entrainment.*

PETER THOMAS
PETER J. GIERASCH
*Center for Radiophysics and
Space Research, Cornell University,
Ithaca, New York 14853*

One of the major geologic processes on Mars is the entrainment and transportation of dust by winds, but spacecraft observations of the genesis and development of local and global dust storms on Mars are sparse (*1*), and the specific conditions necessary for dust entrainment are poorly known (*2*). It has long been suspected that dust devils occur on Mars and that they may be important in the initiation of large dust storms or in increasing the general atmospheric dust

Fig. 1. Viking Orbiter images of dust devils. (A) Image 38B25: clear filter; 39°N, 144°W; solar incidence angle (*i*) = 44.7° from the left side of the image. (B) Image 112A25: clear filter; same area as (A); *i* = 76.4°. Comparison shows which features are variable and which are topographic forms. Dust devils are shown by large arrows; small arrowheads show two craters visible in (B). (C) Image 34B01: clear filter; 36°N, 153°W; *i* = 38.6°. Dust devils are identified by arrows.

dust. The last condition required two time-lapsed, high-resolution images of the same area. The first two conditions required use of the feature itself and its shadow to deduce its shape and orientation. Positive detections were made only in high-resolution images (60 to 80 m per pixel) on revolutions 34, 35, and 38 of Viking Orbiter 2 (L_s = 122° to 124°; L_s, aerocentric longitude of the sun) and on revolution 119 of Viking Orbiter 1 (L_s = 139°). Ninety-seven dust devils were documented in the Orbiter 2 coverage of Arcadia Planitia at 33° to 43°N, 148° to 160°W, and two were found at 37°N, 192°W (near Phlegra Montes).

The images containing dust devils were taken at emission angles of only 10° to 27° (which is close to nadir viewing). The shapes of the clouds were thus best determined from the shadows, which provided a cross section along the line of illumination. The shadows followed the shape of the dust cloud in those cases imaged at the largest emission angles. In particular, the shapes of the shadows were consistent only with the clouds extending from the ground and not with clouds separated from the ground and fortuitously aligned with the ends of their shadows. The overall shapes of the clouds were columnar, cone, funnel, or irregular, and they were generally four to ten times as high as they were wide. The only color data for the clouds were for the two observed on revolution 119a. The red to green ratio (λ = 0.59 μm, 0.54 μm) was approximately 1.7, which is consistent with dust but not consistent with condensate clouds.

The heights of the clouds were measured from the shadows to about ± 200 m (Fig. 2A). Nearly two-thirds (61 of 99) of the clouds were between 1.0 and 2.5 km in height; the maximum height was 6.8 km. Widths of the clouds varied greatly (Fig. 2B). The bases of all the clouds were apparently narrow; many shadows were on the order of 1 pixel (70 m) across. The widest areas near the tops of clouds were nearly 1 km across. The visible forms were thus similar to terrestrial dust devils in general structure, with a narrow base and a wider top (7).

The clouds were observed at times and seasons consistent with a near-maximum heating of the ground by insolation. All clouds were imaged at 14 to 15 hours local time in local summer (L_s = 122°, 139°), when the subsolar latitude was within 13° to 20° of the clouds. Under these conditions, surface temperatures probably reached about 265 K in the afternoon and fell to about 180 K at night (8).
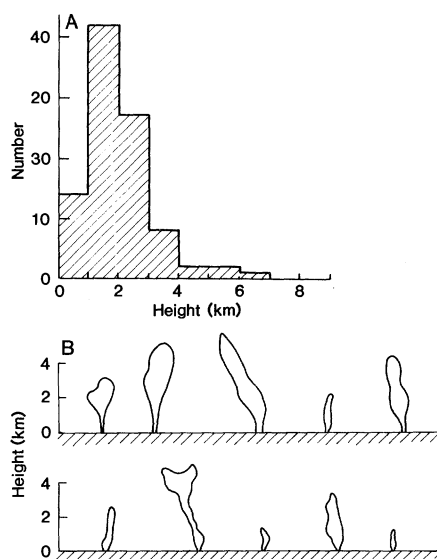

Fig. 2. Sizes and shapes of Martian dust devils. (A) Histogram of heights of dust devils from shadow measurements; accuracy is about ±200 m. Some features that may be 200 to 500 m high are not included because repeat imaging was not of sufficiently high resolution. (B) Sketches of approximate shapes of some clouds as judged from shadows cast with illumination angle of approximately 45°. This projection is close to (but not exactly) that which would be seen from ground level.

Geologically, the dust devils occurred on smooth plains. In Arcadia Planitia dust devils were not seen on the rougher areas composed of outliers of the Olympus Mons (9), which has ridges and knobs 100 to 200 m high and 1 to 5 km long that are spaced on the same scale. The topography of the smoother areas has knobs spaced many kilometers apart and usually much less than 100 m high.

We have made an approximate photometric analysis of the dust clouds and shadows. The brightest parts of the clouds are 5 to 30 percent brighter than the plains, and the shadows are 2 to 10 percent darker. The brightness of the clouds and the darkness of the shadows are closely related. Interpretation of these numbers is difficult because of uncertainties in particle optical properties, but our initial estimates [based on optical properties of the diffuse dust haze on Mars obtained from the Viking landers (10)] indicate that the optical depth along the sun path (incidence angle, 45°) is approximately 0.3 to 0.5. The low contrast of the shadows results from the diffuse brightness of the Mars sky.

We can make a simple estimate of the dust loading. If the particles are 10 μm in diameter and their density is 3 g cm^{-3}, an optical depth of 0.5 requires about 10^{-3} g cm^{-2} along the illumination path. For a path length of 250 m, which is about the

width of the thicker dust devils, this mass implies a loading of approximately 3 × 10^{-8} g cm^{-3}; this is not an unreasonable amount for the atmosphere to carry. A typical dust devil, 2 km high and roughly 200 m in diameter, would contain on the order of 3 × 10^3 kg of dust.

It is difficult to estimate occurrence frequency from the small data sample. The images containing dust devils represent about 3 percent of the total area covered by images with incidence angles less than 50° and resolution better than 150 m per pixel. Elimination of the rougher areas within this set would increase the fractional area that shows dust devils. Quantitative cataloging of rough areas with the global geology map (11) is not practical because the different roughnesses of interest are not discriminated by the global maps. We suspect that the occurrence frequency on smooth terrain near midday and at subsolar or summer latitudes may be high. This conjecture is supported by the observation of dust devils in the Arcadia Planitia region on the 3 days imaged at high resolution (out of 5 days' total time).

The frequency of dust devil occurrence has implications for the structure of the atmospheric boundary layer on Mars, and comparison with Earth may shed light on the dependence of boundary layer structure on the external parameters. Free convection occurs under conditions of light mean wind and strongly heated soil. Near local midday in the summer hemisphere on Mars these conditions should be met frequently (12), and Viking lander measurements have verified this expectation (13). But the most common form of free convection is plumes, which have an aspect (height to width) ratio near unity and show no tight organization or high wind speeds such as those seen for vortices. Plumes are the convective elements that produce the well known "thermals" on Earth. Both observation and theory (14) for Mars show that plumes do not develop sufficiently high velocities to raise dust.

For development of dust devils, the atmospheric convection field must organize into vortices. Necessary conditions for transformation of convection from plumes to vortices are not well understood but are of great importance. One requirement is the presence of vorticity in the flow, although it has been argued that in the case of dust devils the vorticity can originate in the boundary layer itself as vertical shear (15). It has also been argued that the depth of the convection layer is a key quantity and that the relatively thick convective layer on Mars favors vortex formation (16). It is

interesting that predictions of this thickness (14) agree well with the observed heights. Comparative examination of dust devils on Earth and Mars may help clarify many of these issues by demonstrating dependence on different conditions.

Ryan and colleagues (17) have interpreted several events in Viking Lander meteorological records as the probable passage of dust devils. The distinguishing property of these events is a rotating wind vector. Our observations support their interpretation, but simultaneous imaging and meteorological data do not exist for any of the detections. High-resolution imaging coverage is so sparse that occurrence statistics must remain uncertain until better data are obtained.

References and Notes

1. G. A. Briggs, W. A. Baum, J. Barnes, *J. Geophys. Res.* **84**, 2795 (1979).
2. R. Greeley and J. D. Iversen, *Wind as a Geological Process* (Cambridge Univ. Press, Cambridge, 1985).
3. J. A. Ryan, *J. Geophys. Res.* **69**, 3759 (1964); F. M. Neubauer, *ibid.* **71**, 2419 (1966); P. J. Gierasch and R. M. Goody, *J. Atmos. Sci.* **30**, 169 (1973).
4. A. S. Monin and A. M. Yaglom, *Statistical Fluid Mechanics: Mechanics of Turbulence* (Massachusetts Institute of Technology Press, Cambridge, 1965).
5. J. D. Iversen *et al.*, *Icarus* **29**, 381 (1976); R. Greeley *et al.*, *Geophys. Res. Lett.* **7**, 121 (1980); J. B. Pollack *et al.*, *Icarus* **29**, 395 (1976).
6. J. A. Ryan and R. D. Sharman, *J. Geophys. Res.* **86**, 3247 (1981); R. E. Arvidson, E. A. Guinness, H. J. Moore, J. Tillman, S. D. Wall, *Science* **232**, 463 (1983). A dust storm–related wind of 30 m sec^{-1} had the highest of the recorded speeds at the Viking Lander 1 site.
7. J. A. Ryan and J. J. Carroll, *J. Geophys. Res.* **75**, 531 (1970).
8. H. H. Kieffer *et al.*, *ibid.* **82**, 4249 (1977).
9. D. H. Scott, K. L. Tanaka, G. Schaber, *U.S. Geological Survey Map I-1276* (1981).
10. J. B. Pollack *et al.*, *J. Geophys. Res.* **84**, 2929 (1979).
11. D. H. Scott and M. H. Carr, *U.S. Geological Survey Map I-1083* (1978).
12. J. B. Pollack *et al.*, *J. Atmos. Sci.* **38**, 3 (1981).
13. S. L. Hess, *J. Geophys. Res.* **82**, 4559 (1977).
14. J. L. Sutton, C. B. Leovy, J. E. Tillman, *J. Atmos. Sci.* **35**, 2346 (1978); P. J. Gierasch and R. M. Goody, *Planet. Space Sci.* **16**, 615 (1968).
15. T. Maxworthy, *ibid.* **30**, 1717 (1973).
16. R. M. Goody and P. J. Gierasch, *ibid.* **31**, 1021 (1974).
17. J. A. Ryan and R. D. Lucich, *J. Geophys. Res.* **88**, 11005 (1983).
18. Supported by NASA grants NAGW-111 and NGL 33-010-186.

28 May 1985; accepted 8 August 1985

A Potent Nonpeptide Cholecystokinin Antagonist Selective for Peripheral Tissues Isolated from *Aspergillus alliaceus*

Abstract. *A new, competitive, nonpeptide cholecystokinin (CCK) antagonist, asperlicin, was isolated from the fungus* Aspergillus alliaceus. *The compound has 300 to 400 times the affinity for pancreatic, ileal, and gallbladder CCK receptors than proglumide, a standard agent of this class. Moreover, asperlicin is highly selective for peripheral CCK receptors relative to brain CCK and gastrin receptors. Since asperlicin also exhibits long-lasting CCK antagonist activity in vivo, it should provide a valuable tool for investigating the physiological and pharmacological actions of CCK.*

RAYMOND S. L. CHANG
VICTOR J. LOTTI
Department of Microbial Pharmacometrics, Merck Sharp & Dohme Research Laboratories, West Point, Pennsylvania 19486
RICHARD L. MONAGHAN
JEROME BIRNBAUM
EDWARD O. STAPLEY
Department of Microbiology, Merck Sharp & Dohme Research Laboratories, Rahway, New Jersey 07065
MICHAEL A. GOETZ
GEORG ALBERS-SCHÖNBERG
ARTHUR A. PATCHETT
Department of New Lead Discovery, Merck Sharp & Dohme Research Laboratories, Rahway
JERROLD M. LIESCH
OTTO D. HENSENS
JAMES P. SPRINGER
Departments of Analytical Natural Products Chemistry and Biophysics, Merck Sharp & Dohme Research Laboratories, Rahway

Research has been accelerating in recent years on the discovery, mechanism of action, and function of neuropeptides (1). Nonpeptide agonists and antagonists of neuropeptides are being sought to aid studies of their physiological functions and ultimately to provide leads for potential therapeutic developments. We re-
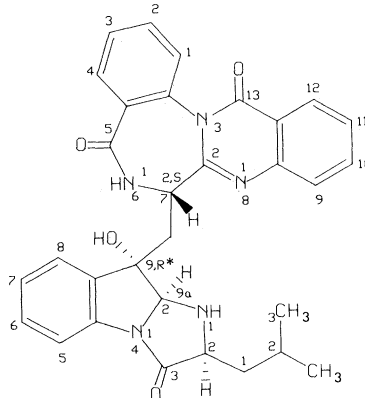

Fig. 1. Structure of asperlicin.

port now the discovery from a microbial source of a potent, competitive, nonpeptide antagonist of the classic gastrointestinal transmitter cholecystokinin (CCK).

CCK is a hormonal regulator of pancreatic and gastric secretion, contraction of the gallbladder, and gut motility (2). CCK also exists in the brain and may have an equally important role as a central nervous system transmitter (3). However, in spite of the potential therapeutic utilities for CCK antagonists, previously reported nonpeptide antagonists such as proglumide, dibutyryl guanosine 3′,5′-cyclic monophosphate (dibutyryl cyclic GMP), and benzotript exhibit only low in vitro potencies, which limit their in vivo usefulness (4). Some peptide fragments of CCK have exhibited greater in vitro potency as CCK antagonists (5), but are subject in vivo to rapid degradation in physiological fluids (6).

Our new CCK antagonist, asperlicin, was isolated from an *Aspergillus alliaceus* strain which has been deposited at the American Type Culture Collection with accession number ATCC 20655 (7). The structure of asperlicin (Fig. 1) was determined by mass spectrometry, nuclear magnetic resonance, and x-ray crystallography (8). Its chemical designation is [2S-[2α,9β,9(R*),9aβ]]-6,7-dihydro-7-[[2,3,9,9a-tetrahydro-9-hydroxy-2-(2-methylpropyl)-3-oxo-1H-imidazo[1,2-a]indol-9-yl]methyl]-quinazolino[3,2-a][1,4]benzodiazepine-5,13-dione. To our knowledge asperlicin is the first nonpeptide antagonist of a neuropeptide to have been isolated from microbial sources.

Asperlicin was compared with known CCK antagonists for its ability to displace the specific binding of ^{125}I-labeled CCK-33 to CCK receptors in rat pancreatic tissue (9). All agents inhibited the specific binding of CCK in a concentration-related manner. The concentration of asperlicin causing half-maximal inhibition of binding (IC$_{50}$ = 1.4 μM) was considerably less than those of the nonpeptide CCK antagonists proglumide, benzotript, and dibutyryl cyclic GMP and similar to the potent peptide antagonist N-carbobenzoxy-CCK-(27-32) (Table 1). The specific binding of ^{125}I-labeled CCK to guinea pig brain tissues (9) and of ^{125}I-labeled gastrin to guinea pig gastric glands (10) was not affected by asperlicin at concentrations 70 times its IC$_{50}$ for inhibiting pancreatic ^{125}I-labeled CCK binding; this result indicates a high degree of selectivity for peripheral CCK receptors.

To examine the mechanism by which asperlicin inhibits CCK binding in pancreatic tissue, ^{125}I-labeled CCK binding